MECSOL Joinville 2017
April 26-28, 2017
Joinville, Santa Catarina, Brazil

Performance of the Weak-form Collocation Meshless Formulation

Tiago da Silva Oliveira
Department of Civil and Environmental Engineering
University of Brasilia
tiago_antuney@hotmail.com

Artur Portela
Department of Civil and Environmental Engineering
University of Brasilia
aportela@unb.br

ABSTRACT

This paper is concerned with the overall performance of the weak-form collocation, a new local meshless method, for solving two-dimensional linear elastic problems when compared to other meshless methods. Four methods are compared in this study, namely, the Generalized-Strain Mesh-free (GSMF) formulation, also known as the weak-form collocation meshless formulation; the Rigid-body Displacement Mesh-free (RBDMF) formulation, the Element-free Galerkin (EFG) and the Meshless Local Petrov-Galerkin Finite Volume Method (MLPG FVM). While the RBDMF, EFG and MLPG FVM rely on integration and quadrature process to obtain the stiffness matrix, the GSMF is completely integration-free, working as a weighted-residual weak-form collocation. This weak-form collocation readily overcomes the well-known difficulties of the strong-form collocation, such as low accuracy and instability of the solution. A numerical example was analyzed with these methods, in order to assess the accuracy, the computational effort and the convergence rate. The results obtained with all methods are in agreement with those of the available analytical solution. The numerical results show that the GSMF, when compared to the other methods, is superior regarding the computational efficiency and accuracy, leading to remarkable results using only one collocation point on each boundary of the local domain.

Keywords: Local Meshless, Generalized-strain, Weak-form collocation, Element-free Galerkin, Meshless Local Petrov-Galerkin.

1. INTRODUCTION

The meshless methods or meshfree methods have intrinsic advantages over the element-based approaches, mostly due to the elimination of the mesh and the high-order continuity of the trial functions. The main feature of these methods is that only a set of scattered nodes in the physical domain is required to approximate the solutions, and the nodes do not need to be connected to form closed polygons. In contrast with the finite element method, the meshless methods can save the pre-processing cost of mesh generation, as no element is required for the whole model [1]. In general, their formulation is based in the weighted-residual method [2].

Therefore, the meshless methods have become an important tool in computational solid mechanics, especially for solving the problems with severe distortion, discontinuities and moving boundaries.

Although the meshless methods have received much attention in recent years, the initiation of their application returns to the late 1970s with the Smooth Particle Hydrodynamics (SPH) for simulat-

ing astrophysical phenomena [3]. The Diffuse Element Method (DEM) increased the publication of meshfree methods based on a weighted-residual weak-form formulation [4]. Later, the Reproducing Kernel Particle Method (RKPM) [5] and the Element-free Galerkin (EFG) method [6] were the first weak-form meshless methods applied in solid mechanics.

All these weak-form meshless methods rely on background cells for the integration of the weighted-residual weak form over the global domain, in the process of the generation of the system of algebraic equations and therefore, they are not truly meshless methods.

To avoid the general background mesh generation, a class of meshfree methods based on local weighted-residual weak forms, such as the Meshless Local Petrov–Galerkin (MLPG) method [7, 8], the Meshless Local Boundary Integral Equation (MLBIE) method [9], the Local Point Interpolation Method (LPIM) [10] and the Local Radial Point Interpolation Method (LRPIM) [11], have been developed. The most popular of these methods is the MLPG, based on a moving least-squares (MLS) approximation. The main difference of the MLPG method to other global meshless methods, such as EFG or RKPM, is that local weak forms are used for integration on overlapping regular-shaped local subdomains, instead of global weak forms and consequently the method does not require the use of a background global mesh, but only a background local grid, which usually has a simple shape.

The MLPG method has been used in solving various engineering problems such as steady convection–diffusion problems [12], incompressible Navier–Stokes problems [13], elastostatics in a homogeneous solid [14] and non-homogeneous solids [15].

An implementation of the meshless Finite Volume Method (FVM) through the MLPG mixed approach was presented in [16] for solving elasto-static problems. In this approach, both the strains and displacements are independently interpolated, at randomly distributed points in the domain, through a local meshless interpolation schemes, in this case the MLS. Then, the nodal values of strains are expressed in terms of the interpolated nodal values of displacements, by simply enforcing the strain-displacement relationships directly by collocation at the nodal points. This formulation eliminates the expensive process of directly differentiating the MLS interpolations for displacements in the entire domain to compute the strains, leading to a high computational efficiency.

Two new formulations were proposed in order to further improve the computational efficiency, the Rigid-body Displacement Mesh-free (RBDMF) formulation and the Generalized-Strain Mesh-free (GSMF) formulation [17]. In the first formulation, the local work theorem leads to a weak form that is a regular local boundary integral equation. In the second formulation, the local work theorem generates a weak form that is completely integration free, working as a weighted-residual weak-form collocation, leading to accurate results without compromising the computational efficiency.

In the present paper a numerical comparison between the weak-form collocation and three other meshless methods, namely the RBDMF, the EFG and the MLPG FVM is performed, for the solution of two-dimensional problems in linear elasticity. The results obtained in this study shows that the GSMF performs better than the other meshless methods regarding both computational efficiency and accuracy, as can be seen in section 6. It is expected that the GSMF framework will be implemented in a variety of problems, including large deformations and fracture mechanics, in the very near future.

2. MLS APPROXIMATION

Let Ω be the domain of a body with boundary Γ and let $N = \{\mathbf{x}_1, \mathbf{x}_2, ..., \mathbf{x}_N\} \in \Omega$ be a set of scattered nodal points that represents a meshless discretization, in which some of them are located on the boundary Γ, where Ω_s, represented as Ω_P, Ω_Q and Ω_R, is the local compact support of a node $\mathbf{x}_i$, represented as $\mathbf{x}_P$, $\mathbf{x}_Q$ and $\mathbf{x}_R$; $\Omega_\mathbf{x}$ is the domain of definition of a sampling point $\mathbf{x}$ and Ω_q is the local weak-form domain or quadrature domain of a node $\mathbf{x}_i$, as represented in Fig. 1.

Circular or rectangular local supports, centered at each nodal point, can be used. In a neighborhood of a sampling point $\mathbf{x}$, the domain of definition of MLS approximation is the subdomain $\Omega_\mathbf{x}$, where

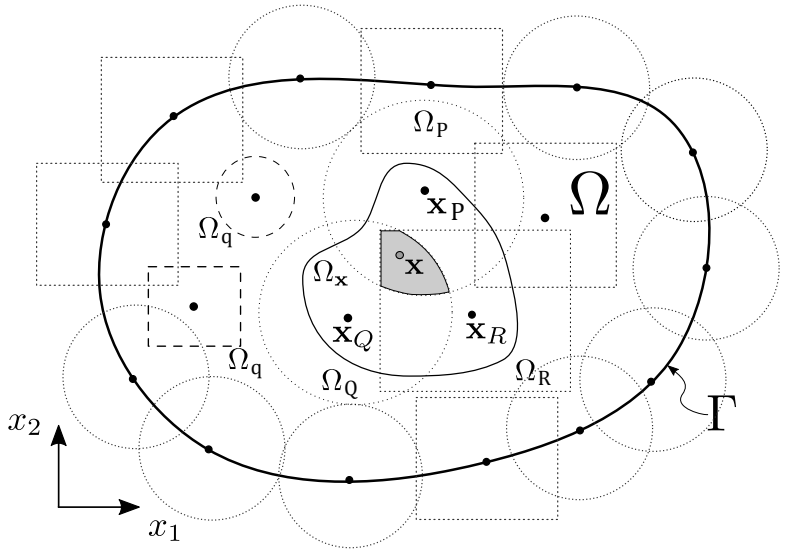

Figure 1. Representation of a global domain Ω and boundary Γ in a meshless discretization, with $\mathbf{x}_i$ nodes distributed within the body.

the approximation is defined.

2.1 Shape Functions

Let $\Omega_\mathbf{x}$ be the domain of definition of the MLS approximation, in a neighbourhood of a sampling point $\mathbf{x}$. To approximate the displacement $u(\mathbf{x}) \in \Omega_\mathbf{x}$, over a number of scattered nodes $\mathbf{x}_i \in \Omega$, $i = 1,2,\ldots,n$, where the nodal parameters $\hat{u}_i$ are defined, the MLS approximation is given by

$$u^h(\mathbf{x}) = \mathbf{p}^T(\mathbf{x})\mathbf{a}(\mathbf{x}), \tag{1}$$

for $\mathbf{x} \in \Omega_\mathbf{x}$, in which

$$\mathbf{p}^T(\mathbf{x}) = [p_1(\mathbf{x}), p_2(\mathbf{x}), \ldots, p_m(\mathbf{x})], \tag{2}$$

is a vector of the complete monomial basis of order m and $\mathbf{a}(\mathbf{x})$ is the vector of unknown coefficients $a_j(\mathbf{x})$, $j = 1,2,\ldots,m$ that are functions of the space coordinates $\mathbf{x} = [x_1, x_2]^T$, for 2-D problems.

The coefficient vector $\mathbf{a}(\mathbf{x})$ is determined by minimizing the weighted discrete L_2 norm

$$J(\mathbf{x}) = \frac{1}{2}\sum_{i=1}^{n} w_i(\mathbf{x}) \left[u^h(\mathbf{x_i}) - \hat{u}_i\right]^2 = \frac{1}{2}\sum_{i=1}^{n} w_i(\mathbf{x}) \left[\mathbf{p}^T(\mathbf{x}_i)\mathbf{a}(\mathbf{x}) - \hat{u}_i\right]^2, \tag{3}$$

with respect to each term of $\mathbf{a}(\mathbf{x})$, in which $w_i(\mathbf{x})$ is the weight function associated with the node $\mathbf{x}_i$, with compact support that is $w_i(\mathbf{x}) > 0$, for all $\mathbf{x}$ in the support of $w_i(\mathbf{x})$. Figure 1 represents schematically the compact support of the MLS weight functions associated with a few nodes. Finding the extremum of $J(\mathbf{x})$ with respect to each term of $\mathbf{a}(\mathbf{x})$, leads to

$$\mathbf{A}(\mathbf{x})\mathbf{a}(\mathbf{x}) = \mathbf{B}(\mathbf{x})\hat{\mathbf{u}}, \tag{4}$$

in which

$$\mathbf{A}(\mathbf{x}) = \sum_{i=1}^{n} w_i(\mathbf{x})\mathbf{p}(\mathbf{x}_i)\mathbf{p}^T(\mathbf{x}_i), \tag{5}$$

$$\mathbf{B}(\mathbf{x}) = [w_1(\mathbf{x})\mathbf{p}(\mathbf{x}_1), w_2(\mathbf{x})\mathbf{p}(\mathbf{x}_2), \ldots, w_n(\mathbf{x})\mathbf{p}(\mathbf{x}_n)] \tag{6}$$

and

$$\hat{\mathbf{u}} = [\hat{u}_1, \hat{u}_2, \ldots, \hat{u}_n]. \tag{7}$$

Solving Eq. (4) for $\mathbf{a}(\mathbf{x})$ yields

$$\mathbf{a}(\mathbf{x}) = \mathbf{A}^{-1}(\mathbf{x})\mathbf{B}(\mathbf{x})\hat{\mathbf{u}}, \tag{8}$$

provided $n \geq m$, for each sampling point $\mathbf{x}$, as a necessary condition for a well-defined MLS approximation. In the end, substituting for $\mathbf{a}(\mathbf{x})$ into Eq. (1) results in the MLS approximation

$$u^h(\mathbf{x}) = \sum_{i=1}^{n} \phi_i(\mathbf{x})\hat{u}_i, \tag{9}$$

in which

$$\phi_i(\mathbf{x}) = \sum_{j=1}^{m} p_j(\mathbf{x}) \left[\mathbf{A}^{-1}(\mathbf{x})\mathbf{B}(\mathbf{x})\right]_{ji} \tag{10}$$

is the shape function of the MLS approximation corresponding to the node $\mathbf{x}_i$, schematically represented in Fig. 2. The MLS shape functions are not nodal interpolants that is $\phi_i(\mathbf{x}_j) \neq \delta_{ij}$. The local

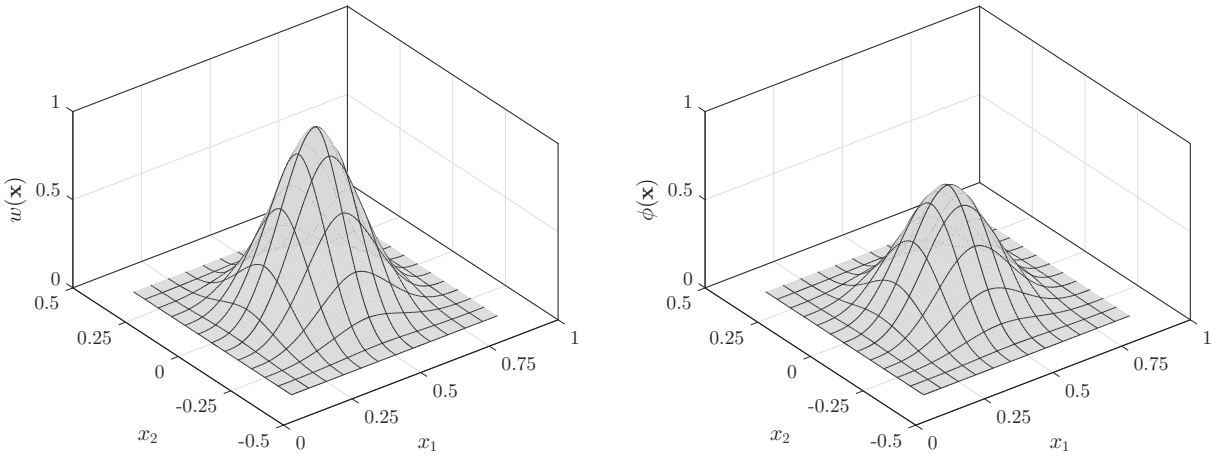

Figure 2. Respectively the typical weight function and shape function of the MLS approximation.

character of the MLS approximation is preserved, since $\phi_i(\mathbf{x})$ vanishes for $\mathbf{x}$ not in the local domain of the node $\mathbf{x}_i$. The nodal shape function is complete up to the order of the basis. Also, the smoothness of the nodal shape function is determined by the smoothness of the basis and of the weight function. The spatial derivatives of the shape function $\phi_i(\mathbf{x})$ are given by

$$\phi_{i,k} = \sum_{j=1}^{m} \left[p_{j,k}(\mathbf{A}^{-1}\mathbf{B})_{ji} + p_j(\mathbf{A}^{-1}\mathbf{B}_{,k} - \mathbf{A}^{-1}\mathbf{A}_{,k}\mathbf{A}^{-1}\mathbf{B})_{ji}\right], \tag{11}$$

in which $()_{,k} = \partial()/\partial x_k$.

2.2 Weight Functions

Weight functions $w_i(\mathbf{x})$, schematically represented in Fig. 2, firstly introduced in Eq. (3) for each node $\mathbf{x}_i$, have a compact support which defines the subdomain where $w_i(\mathbf{x}) > 0$, for all sampling point

x. For the sake of simplicity, this paper considers rectangular compact supports with weight functions defined as

$$w_i(\mathbf{x}) = w_{i_x}(\mathbf{x})\, w_{i_y}(\mathbf{x}) \tag{12}$$

with the weight function given by the quartic spline function

$$w_{i_x}(\mathbf{x}) = \begin{cases} 1 - 6\left(\dfrac{d_{i_x}}{r_{i_x}}\right)^2 + 8\left(\dfrac{d_{i_x}}{r_{i_x}}\right)^3 - 3\left(\dfrac{d_{i_x}}{r_{i_x}}\right)^4 & \text{for } 0 \le d_{i_x} \le r_{i_x} \\ 0 & \text{for } d_{i_x} > r_{i_x} \end{cases} \tag{13}$$

and

$$w_{i_y}(\mathbf{x}) = \begin{cases} 1 - 6\left(\dfrac{d_{i_y}}{r_{i_y}}\right)^2 + 8\left(\dfrac{d_{i_y}}{r_{i_y}}\right)^3 - 3\left(\dfrac{d_{i_y}}{r_{i_y}}\right)^4 & \text{for } 0 \le d_{i_y} \le r_{i_y} \\ 0 & \text{for } d_{i_y} > r_{i_y}, \end{cases} \tag{14}$$

in which $d_{i_x} = \|x - x_i\|$ and $d_{i_y} = \|y - y_i\|$. The parameters r_{i_x} and r_{i_y} represent the size of the support for the node i, respectively in the x and y directions.

2.3 Elastic Field

The elastic field is now approximated at a sampling point **x**. Considering Eq. (9), displacement and strain components are respectively approximated as

$$\mathbf{u} = \begin{bmatrix} u^h(\mathbf{x}) \\ v^h(\mathbf{x}) \end{bmatrix} = \begin{bmatrix} \phi_1(\mathbf{x}) & 0 & \dots & \phi_n(\mathbf{x}) & 0 \\ 0 & \phi_1(\mathbf{x}) & \dots & 0 & \phi_n(\mathbf{x}) \end{bmatrix} \begin{bmatrix} \hat{u}_1 \\ \hat{v}_1 \\ \vdots \\ \hat{u}_n \\ \hat{v}_n \end{bmatrix} = \mathbf{\Phi}\,\hat{\mathbf{u}} \tag{15}$$

and

$$\boldsymbol{\varepsilon} = \mathbf{L}\,\mathbf{u} = \mathbf{L}\,\mathbf{\Phi}\,\hat{\mathbf{u}} = \mathbf{B}\,\hat{\mathbf{u}}, \tag{16}$$

in which geometrical linearity is assumed in the differential operator **L** and thus,

$$\mathbf{B} = \begin{bmatrix} \phi_{1,1} & 0 & \dots & \phi_{n,1} & 0 \\ 0 & \phi_{1,2} & \dots & 0 & \phi_{n,2} \\ \phi_{1,2} & \phi_{1,1} & \dots & \phi_{n,2} & \phi_{n,1} \end{bmatrix}. \tag{17}$$

Stress and traction components are respectively approximated as

$$\boldsymbol{\sigma} = \mathbf{D}\,\boldsymbol{\varepsilon} = \mathbf{D}\,\mathbf{B}\,\hat{\mathbf{u}} \tag{18}$$

and

$$\mathbf{t} = \mathbf{n}\,\boldsymbol{\sigma} = \mathbf{n}\,\mathbf{D}\,\mathbf{B}\,\hat{\mathbf{u}}, \tag{19}$$

in which **D** is the matrix of the elastic constants and **n** is the matrix of the components of the unit outward normal, defined as

$$\mathbf{n} = \begin{bmatrix} n_1 & 0 & n_2 \\ 0 & n_2 & n_1 \end{bmatrix}. \tag{20}$$

Equations (15) to (19) show that, at a sampling point $\mathbf{x} \in \Omega_{\mathbf{x}}$, the variables of the elastic field are defined in terms of the nodal unknowns $\hat{\mathbf{u}}$.

3. LOCAL FORM OF THE WORK THEOREM

This section present the development of the local form of the work theorem, first introduced in [17].

Let Ω be the domain of a body and Γ its boundary, subdivided in Γ_u and Γ_t that is $\Gamma = \Gamma_u \cup \Gamma_t$; nodal points P, Q and R have corresponding local domains Ω_P, Ω_Q and Ω_R, as represented in Fig. 3. The mixed fundamental boundary value problem of linear elastostatics aims to determine the

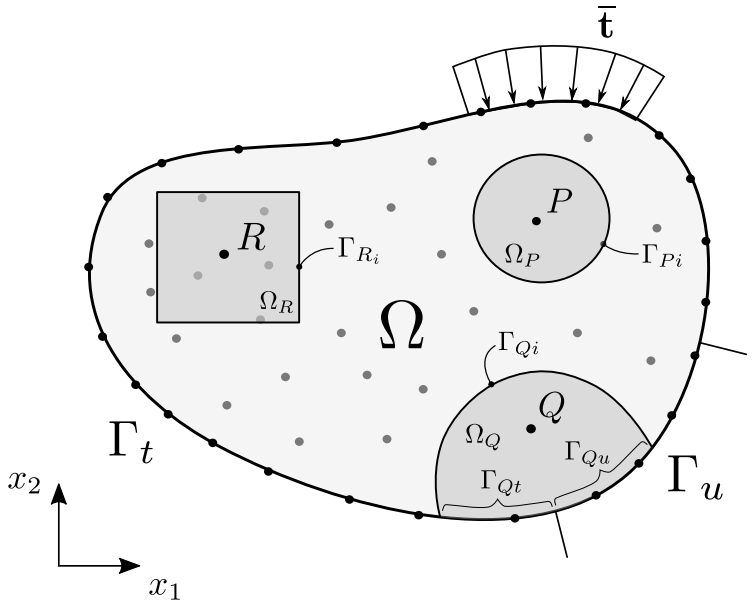

Figure 3. Meshless discretization of the global domain Ω and the local domains Ω_P, Ω_Q and Ω_R, with boundary $\Gamma = \Gamma_u \cup \Gamma_t$ represented.

distribution of stresses σ, strains ε and displacements $\mathbf{u}$ throughout the body, when it has constrained displacements $\bar{\mathbf{u}}$ defined on Γ_u and is loaded by an external system of distributed surface and body forces with densities denoted by $\bar{\mathbf{t}}$ on Γ_t and $\mathbf{b}$ in Ω, respectively.

A totally admissible elastic field is the solution of the posed problem that simultaneously satisfies the kinematic admissibility and the static admissibility. If this solution exists, it can be shown that it is unique, provided linearity and stability of the material are admitted [18, 19].

The general work theorem establishes an energy relationship between any statically-admissible stress field and any kinematically-admissible strain field that can be defined in the body. Derived as a weighted residual statement, the work theorem serves as a unifying basis for the formulation of numerical models in Continuum Mechanics [20].

In the domain of the body, consider a statically-admissible stress field that is

$$\mathbf{L}^T \sigma + \mathbf{b} = \mathbf{0}, \tag{21}$$

in the domain Ω, with boundary conditions

$$\mathbf{t} = \mathbf{n}\,\sigma = \bar{\mathbf{t}}, \tag{22}$$

on the static boundary Γ_t, in which the vector σ represents the stress components; $\mathbf{L}$ is a matrix differential operator; the vector $\mathbf{t}$ represent the traction components; $\bar{\mathbf{t}}$ represent prescribed values of tractions and $\mathbf{n}$ represents the outward unit normal components to the boundary.

In the global domain Ω, consider an arbitrary local subdomain Ω_Q, centered at the point Q, with boundary $\Gamma_Q = \Gamma_{Qi} \cup \Gamma_{Qt} \cup \Gamma_{Qu}$, in which Γ_{Qi} is the interior local boundary, while Γ_{Qt} and Γ_{Qu}

are local boundaries that respectively share a global boundary, as represented in Fig. 3. Due to its arbitrariness, this local domain can be overlapping with other similar subdomains. For the local domain Ω_Q, the strong form of the weighted-residual equation is written as

$$\int_{\Omega_Q} \left(\mathbf{L}^T \boldsymbol{\sigma} + \mathbf{b}\right)^T \mathbf{W}_\Omega \, \mathrm{d}\Omega + \int_{\Gamma_{Qt}} \left(\mathbf{t} - \bar{\mathbf{t}}\right)^T \mathbf{W}_\Gamma \, \mathrm{d}\Gamma = \mathbf{0}, \tag{23}$$

in which $\mathbf{W}_\Omega$ and $\mathbf{W}_\Gamma$ are arbitrary weighting functions defined, respectively in Ω and on Γ. When the domain term of Eq. (23) is integrated by parts, the following local weak form of the weighted residual equation is obtained

$$\int_{\Gamma_Q} (\mathbf{n}\boldsymbol{\sigma})^T \mathbf{W}_\Omega \, \mathrm{d}\Gamma - \int_{\Omega_Q} \left(\boldsymbol{\sigma}^T \mathbf{L}\mathbf{W}_\Omega - \mathbf{b}^T \mathbf{W}_\Omega\right) \mathrm{d}\Omega + \int_{\Gamma_{Qt}} \left(\mathbf{t} - \bar{\mathbf{t}}\right)^T \mathbf{W}_\Gamma \, \mathrm{d}\Gamma = \mathbf{0} \tag{24}$$

which now requires continuity of $\mathbf{W}_\Omega$, as an admissibility condition for integrability. For the sake of convenience, the arbitrary weighting function $\mathbf{W}_\Gamma$ is chosen as

$$\mathbf{W}_\Gamma = -\mathbf{W}_\Omega, \tag{25}$$

on the boundary Γ_{Qt}. Thus, Eq. (24) leads to

$$\int_{\Gamma_Q - \Gamma_{Qt}} \mathbf{t}^T \mathbf{W}_\Omega \, \mathrm{d}\Gamma + \int_{\Gamma_{Qt}} \bar{\mathbf{t}}^T \mathbf{W}_\Omega \, \mathrm{d}\Gamma - \int_{\Omega_Q} \left(\boldsymbol{\sigma}^T \mathbf{L}\mathbf{W}_\Omega - \mathbf{b}^T \mathbf{W}_\Omega\right) \mathrm{d}\Omega = \mathbf{0}. \tag{26}$$

Consider further an arbitrary kinematically-admissible strain field $\boldsymbol{\varepsilon}^*$, with continuous displacements $\mathbf{u}^*$ and small derivatives, in order to assume geometrical linearity, defined in the global domain that is

$$\boldsymbol{\varepsilon}^* = \mathbf{L}\,\mathbf{u}^*, \tag{27}$$

in the domain Ω, with boundary conditions

$$\mathbf{u}^* = \bar{\mathbf{u}}, \tag{28}$$

on the kinematic boundary Γ_u.

When the continuous arbitrary weighting function $\mathbf{W}_\Omega$, is defined as

$$\mathbf{W}_\Omega = \mathbf{u}^*, \tag{29}$$

the weak form (26), of the weighted residual equation, becomes

$$\int_{\Gamma_Q - \Gamma_{Qt} - \Gamma_{Qu}} \mathbf{t}^T \mathbf{u}^* \, \mathrm{d}\Gamma + \int_{\Gamma_{Qu}} \mathbf{t}^T \bar{\mathbf{u}}^* \, \mathrm{d}\Gamma + \int_{\Gamma_{Qt}} \bar{\mathbf{t}}^T \mathbf{u}^* \, \mathrm{d}\Gamma - \int_{\Omega_Q} \left(\boldsymbol{\sigma}^T \mathbf{L}\mathbf{u}^* - \mathbf{b}^T \mathbf{u}^*\right) \mathrm{d}\Omega = \mathbf{0} \tag{30}$$

which can be written in a compact form as

$$\int_{\Gamma_Q} \mathbf{t}^T \mathbf{u}^* \, \mathrm{d}\Gamma + \int_{\Omega_Q} \mathbf{b}^T \mathbf{u}^* \, \mathrm{d}\Omega = \int_{\Omega_Q} \boldsymbol{\sigma}^T \boldsymbol{\varepsilon}^* \, \mathrm{d}\Omega. \tag{31}$$

This equation is the starting point of the kinematically admissible formulations of the local mesh-free methods presented in this paper. Equation (31) which expresses the static-kinematic duality, is the local form of the well-known work theorem, the fundamental identity of solid mechanics [21].

It is important to notice that the stress field σ, is any one that satisfies equilibrium with the applied external forces $\mathbf{b}$ and $\mathbf{t}$, which is not necessarily the stress field that actually settles in the body. Also, the strain field ε^*, is any one that is compatible with the constraints $\mathbf{u}^* = \overline{\mathbf{u}}$, which is not necessarily the strain field that actually settles in the body. This two fields are not connected by any constitutive relationship; indeed, as a consequence of the arbitrariness of the weighting function $\mathbf{W}_\Omega$ they are completely independent. For that reason Eq. (31) can be used under the only assumption of geometrical linearity.

It is the independence of the two admissible fields of the Eq. (31) that allows the generation of different meshfree methods, when the strain field is locally defined through different options, as carried out in this paper.

A final important remark, worth of mentioning, is that the local domain Ω_Q, is any arbitrary subdomain of the global domain Ω, of the body.

4. MODELING STRATEGY

Different formulations of local meshfree methods can be derived when the arbitrary kinematically-admissible field ε^*, is locally defined in the work theorem, Eq. (31). In the following section, simple kinematically-admissible local fields will be used to derive the meshless formulation presented in this paper, the Generalized-Strain Mesh-Free (GSMF) formulation.

On the other hand, the statically-admissible local field σ, will be always assumed as the elastic field that actually settles in the body. Not only satisfying static admissibility, through Eq. (21) and (22), but also satisfying kinematic admissibility in this elastic field defined as

$$\varepsilon = \mathbf{L}\,\mathbf{u}, \tag{32}$$

in the domain Ω, with boundary conditions

$$\mathbf{u} = \overline{\mathbf{u}}, \tag{33}$$

on the kinematic boundary Γ_u; in which the displacements $\mathbf{u}$, are assumed continuous with small derivatives, in order to allow for geometrical linearity of the strain field ε. Therefore, Eq. (33) must be enforced in the numerical model, in order to provide a unique solution of the posed problem.

For a meshless discretization of the body, the local weak-form domain or quadrature domain Ω_Q, centered at a node Q, can be defined in this paper as a rectangular or circular subdomain, as represented in Fig. 3.

5. GENERALIZED-STRAIN FORMULATION

This section briefly discuss the development of the Generalized-Strain Mesh-free (GSMF) formulation. For the complete and detailed development see [17].

In the local form of the work theorem, Eq. (31), the kinematically-admissible displacement field $\mathbf{u}^*$, was assumed as a continuous function leading to a regular integrable function that is the kinematically-admissible strain field ε^*. However, this continuity assumption on $\mathbf{u}^*$, enforced in the local form of the work theorem, is not absolutely required but can be relaxed by convenience, provided ε^* can be useful as a generalized function, in the sense of the theory of distributions [22]. Hence, this formulation considers that the kinematically-admissible displacement field is a piecewise continuous function, defined in terms of the Heaviside step function and therefore the corresponding kinematically-admissible strain field is a generalized function, defined in terms of the Dirac delta function.

For the sake of the simplicity, in dealing with Heaviside and Dirac delta functions in a two-

dimensional coordinate space, consider a scalar function d, defined as

$$d = \| \mathbf{x} - \mathbf{x}_Q \| \quad \text{that is} \quad \begin{cases} d = 0 & \text{if } \mathbf{x} \equiv \mathbf{x}_Q \\ d > 0 & \text{if } \mathbf{x} \neq \mathbf{x}_Q, \end{cases} \tag{34}$$

which represents the absolute-value function of the distance between a field point $\mathbf{x}$ and a particular reference point $\mathbf{x}_Q$, in the local domain $\Omega_Q \cup \Gamma_Q$ assigned to the field node Q. Therefore, this definition always assumes $d = d(\mathbf{x}, \mathbf{x}_Q) \geq 0$, as a positive or null value, in this case whenever $\mathbf{x}$ and $\mathbf{x}_Q$ are coincident points. It is important to remark that, in Eq. (34), neither the field point $\mathbf{x}$ nor the reference point $\mathbf{x}_Q$ is necessarily a nodal point of the local domain.

For a scalar coordinate $d \supset d(\mathbf{x}, \mathbf{x}_Q)$, the Heaviside step function can be defined as

$$H(d) = \begin{cases} 1 & \text{if } d \leq 0 \ (d = 0 \text{ for } \mathbf{x} \equiv \mathbf{x}_Q), \\ 0 & \text{if } d > 0 \text{ that is } \mathbf{x} \neq \mathbf{x}_Q, \end{cases} \tag{35}$$

in which the discontinuity is assumed at $\mathbf{x}_Q$ and consequently, the Dirac delta function is defined with the following properties

$$\delta(d) = H'(d) = \begin{cases} \infty & \text{if } d = 0 \text{ that is } \mathbf{x} \equiv \mathbf{x}_Q, \\ 0 & \text{if } d \neq 0 \ (d > 0 \text{ for } \mathbf{x} \neq \mathbf{x}_Q) \end{cases} \quad \text{and} \quad \int_{-\infty}^{+\infty} \delta(d) \, \mathrm{d}d = 1, \tag{36}$$

in which $H'(d)$ represents the distributional derivative of $H(d)$. Note that the derivative of $H(d)$, with respect to the coordinate x_i, can be defined as

$$H(d)_{,i} = H'(d) \, d_{,i} = \delta(d) \, d_{,i} = \delta(d) \, n_i. \tag{37}$$

Since the result of this equation is not affected by any particular value of the constant n_i, this constant will be conveniently redefined later on.

Now Consider that d_l, d_j and d_k represent the distance function d, defined in Eq. (34), for corresponding collocation points $\mathbf{x}_l$, $\mathbf{x}_j$ and $\mathbf{x}_k$. Then, when Eq. (34) to (36) are considered, the displacement field $\mathbf{u}^*(\mathbf{x})$, can be conveniently defined as

$$\mathbf{u}^*(\mathbf{x}) = \left[\frac{L_i}{n_i} \sum_{l=1}^{n_i} H(d_l) + \frac{L_t}{n_t} \sum_{j=1}^{n_t} H(d_j) + \frac{S}{n_\Omega} \sum_{k=1}^{n_\Omega} H(d_k) \right] \mathbf{e}, \tag{38}$$

in which $\mathbf{e} = [1 \ \ 1]^T$ represents the metric of the orthogonal directions and n_i, n_t and n_Ω represent the number of collocation points, respectively on the local interior boundary $\Gamma_{Qi} = \Gamma_Q - \Gamma_{Qt} - \Gamma_{Qu}$ with length L_i, on the local static boundary Γ_{Qt} with length L_t and in the local domain Ω_Q with area S. This assumed displacement field $\mathbf{u}^*(\mathbf{x})$, a discrete rigid-body unit displacement defined at collocation points, is schematically represented in Fig. 4.

Therefore, when Eq. (37) are taken into account, the strain field $\boldsymbol{\varepsilon}^*(\mathbf{x})$, is given by

$$\begin{aligned} \boldsymbol{\varepsilon}^*(\mathbf{x}) = \mathbf{L}\mathbf{u}^*(\mathbf{x}) &= \left[\frac{L_i}{n_i} \sum_{l=1}^{n_i} \mathbf{L}H(d_l) + \frac{L_t}{n_t} \sum_{j=1}^{n_t} \mathbf{L}H(d_j) + \frac{S}{n_\Omega} \sum_{k=1}^{n_\Omega} \mathbf{L}H(d_k) \right] \mathbf{e} = \\ &= \left[\frac{L_i}{n_i} \sum_{l=1}^{n_i} \boldsymbol{\delta}(d_l)\mathbf{n}^T + \frac{L_t}{n_t} \sum_{j=1}^{n_t} \boldsymbol{\delta}(d_j)\mathbf{n}^T + \frac{S}{n_\Omega} \sum_{k=1}^{n_\Omega} \boldsymbol{\delta}(d_k)\mathbf{n}^T \right] \mathbf{e}, \end{aligned} \tag{39}$$

in which $\mathbf{n}$ is given by Eq. (20), with arbitrary components n_i that will be defined later on.

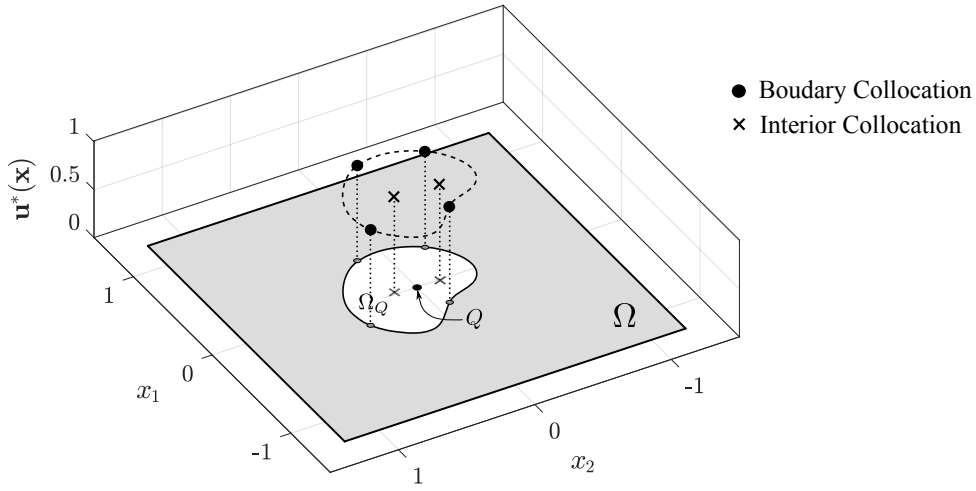

Figure 4. Schematic representation of the displacement $\mathbf{u}^*(\mathbf{x})$ of Eq. (38), a discrete rigid-body unit displacement defined at collocation points, of the Generalized-Strain Mesh-free formulation, for a local domain associated with a field node Q.

Having defined the displacement and the strain components of the kinematically-admissible field, respectively with Eq. (38) and (39), the local work theorem, Eq. (31), can be written as

$$\int_{\Gamma_Q - \Gamma_{Qt}} \mathbf{t}^T \mathbf{u}^* \, \mathrm{d}\Gamma + \int_{\Gamma_{Qt}} \bar{\mathbf{t}}^T \mathbf{u}^* \, \mathrm{d}\Gamma + \int_{\Omega_Q} \mathbf{b}^T \mathbf{u}^* \, \mathrm{d}\Omega = \int_{\Omega_Q} \sigma^T \varepsilon^* \, \mathrm{d}\Omega \tag{40}$$

that is

$$\begin{aligned} \frac{L_i}{n_i} \sum_{l=1}^{n_i} \int_{\Gamma_Q - \Gamma_{Qt}} \mathbf{t}^T H(d_l) \mathbf{e} \, \mathrm{d}\Gamma + \frac{L_t}{n_t} \sum_{j=1}^{n_t} \int_{\Gamma_{Qt}} \bar{\mathbf{t}}^T H(d_j) \mathbf{e} \, \mathrm{d}\Gamma + \frac{S}{n_\Omega} \sum_{k=1}^{n_\Omega} \int_{\Omega_Q} \mathbf{b}^T H(d_k) \mathbf{e} \, \mathrm{d}\Omega = \\ = \frac{S}{n_\Omega} \sum_{k=1}^{n_\Omega} \int_{\Omega_Q} \sigma^T \delta(d_k) \mathbf{n}^T \mathbf{e} \, \mathrm{d}\Omega. \end{aligned} \tag{41}$$

Taking into account the properties of the Heaviside step function, defined in Eq. (35), Eq. (41) simply leads to

$$\mathbf{e}^T \left[\frac{L_i}{n_i} \sum_{l=1}^{n_i} \mathbf{t}_{\mathbf{x}_l} + \frac{L_t}{n_t} \sum_{j=1}^{n_t} \bar{\mathbf{t}}_{\mathbf{x}_j} + \frac{S}{n_\Omega} \sum_{k=1}^{n_\Omega} \mathbf{b}_{\mathbf{x}_k} - \frac{S}{n_\Omega} \sum_{k=1}^{n_\Omega} \mathbf{n} \int_{\Omega_Q} \delta(d_k) \sigma \, \mathrm{d}\Omega \right] = \mathbf{0} \tag{42}$$

which, after considering the selective properties of Dirac delta function, leads to

$$\frac{L_i}{n_i} \sum_{l=1}^{n_i} \mathbf{t}_{\mathbf{x}_l} - \frac{S}{n_\Omega} \mathbf{n} \sum_{k=1}^{n_\Omega} \sigma_{\mathbf{x}_k} = - \frac{L_t}{n_t} \sum_{j=1}^{n_t} \bar{\mathbf{t}}_{\mathbf{x}_j} - \frac{S}{n_\Omega} \sum_{k=1}^{n_\Omega} \mathbf{b}_{\mathbf{x}_k}. \tag{43}$$

Finally, when the variable $\mathbf{n}$, given by Eq. (20), is arbitrarily defined with identically null components $n_i = 0$, as allowed by Eq. (37), the Eq. (43) leads to

$$\frac{L_i}{n_i} \sum_{l=1}^{n_i} \mathbf{t}_{\mathbf{x}_l} = - \frac{L_t}{n_t} \sum_{j=1}^{n_t} \bar{\mathbf{t}}_{\mathbf{x}_j} - \frac{S}{n_\Omega} \sum_{k=1}^{n_\Omega} \mathbf{b}_{\mathbf{x}_k}. \tag{44}$$

Equation (44) states the equilibrium of tractions and body forces, pointwisely defined at collocation points, as schematically represented in Fig. 5. It can be seen that this is the pointwise version of

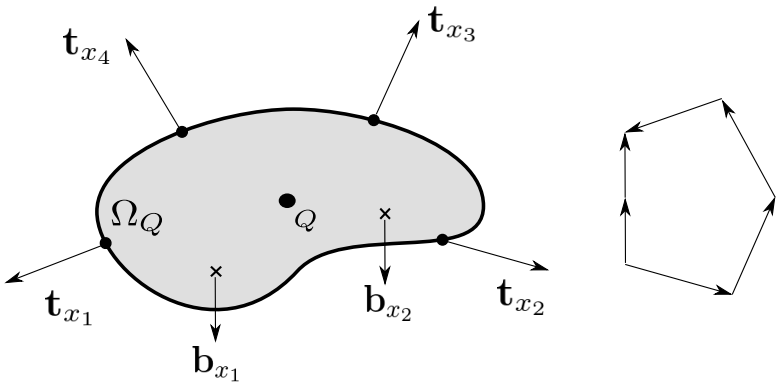

Figure 5. Schematic representation of the equilibrium of tractions and body forces of Eq. (44), pointwisely defined at collocation points of a local domain associated with a field node Q, of the Generalized-Strain Mesh-free formulation.

the Euler - Cauchy stress principle. This is the equation used in the Generalized-Strain Mesh-free (GSMF) formulation which, therefore, is free of integration. Since the work theorem is a weighted-residual weak form, it can be easily seen that this integration-free formulation is nothing else other than a weighted-residual weak-form collocation.

Equations (44), of the Generalized-Strain Mesh-free formulation, can be derived from another kinematically-admissible displacement field, defined as a linear combination of Kronecker delta function evaluations at an arbitrary number of collocation points, conveniently arranged in the local domain $\Omega_Q \cup \Gamma_Q$ of the field node Q, as see in [17].

Discretization of Eq. (44) is carried out with the MLS approximation, Eq. (15) to (19), for the local domain Ω_Q, in terms of the nodal unknowns $\hat{\mathbf{u}}$, thus leading to the system of two linear algebraic equations

$$\frac{L_i}{n_i}\sum_{l=1}^{n_i}\mathbf{n}_{\mathbf{x}_l}\mathbf{D}\mathbf{B}_{\mathbf{x}_l}\hat{\mathbf{u}} = -\frac{L_t}{n_t}\sum_{j=1}^{n_t}\bar{\mathbf{t}}_{\mathbf{x}_j} - \frac{S}{n_\Omega}\sum_{k=1}^{n_\Omega}\mathbf{b}_{\mathbf{x}_k} \tag{45}$$

that can be written as

$$\mathbf{K}_Q\,\hat{\mathbf{u}} = \mathbf{F}_Q, \tag{46}$$

in which $\mathbf{K}_Q$, the nodal stiffness matrix associated with the local domain Ω_Q, is a $2\times 2n$ matrix given by

$$\mathbf{K}_Q = \frac{L_i}{n_i}\sum_{l=1}^{n_i}\mathbf{n}_{\mathbf{x}_l}\mathbf{D}\mathbf{B}_{\mathbf{x}_l} \tag{47}$$

and $\mathbf{F}_Q$ is the respective force vector given by

$$\mathbf{F}_Q = -\frac{L_t}{n_t}\sum_{j=1}^{n_t}\bar{\mathbf{t}}_{\mathbf{x}_j} - \frac{S}{n_\Omega}\sum_{k=1}^{n_\Omega}\mathbf{b}_{\mathbf{x}_k} \tag{48}$$

Consider that the problem has a total of N field nodes Q, each one associated with the respective local region Ω_Q. Assembling Eq. (46), for all M interior and static–boundary field nodes leads to the global system of $2M\times 2N$ equations

$$\mathbf{K}\,\hat{\mathbf{u}} = \mathbf{F}. \tag{49}$$

Finally, the remaining equations are obtained from the $N-M$ boundary field nodes on the kinematic boundary. For a field node on the kinematic boundary, a direct interpolation method is used to impose the kinematic boundary condition as

$$u_k^h(\mathbf{x}_j) = \sum_{i=1}^{n} \phi_i(\mathbf{x}_j)\hat{u}_{ik} = \overline{\mathbf{u}}_k, \tag{50}$$

or, in matrix form as

$$\mathbf{u}_k = \Phi_k \hat{\mathbf{u}} = \overline{\mathbf{u}}_k, \tag{51}$$

with $k = 1,2$, where $\overline{\mathbf{u}}_k$ is the specified nodal displacement component. Equations (50) are directly assembled into the global system of equations (49).

6. NUMERICAL RESULTS

This section presents some numerical results for the cantilever beam, comparing the Generalized-Strain Mesh-free (GSMF) formulation with the Rigid-Body Displacement Mesh-free (RBDMF) formulation, the Element-free Galerkin (EFG) and the Meshless Local Petrov–Galerkin Finite Volume Method (MLPG FVM). But first the effects of the size of support or quadrature domains was investigated.

For a generic node i, the size of the local support Ω_s and the local domain of integration/collocation Ω_q are respectively given by

$$r_{\Omega_s} = \alpha_s c_i, \tag{52}$$

and

$$r_{\Omega_q} = \alpha_q c_i, \tag{53}$$

in which c_i represents the distance of the node i, to the nearest neighboring node.

Usually, the ratio of the local support size r_{Ω_s} is greater than 1.0, to make sure that there are enough points to support the nodes on the global boundary. While the ratio of the sub-domain or local domain of integration/collocation size r_{Ω_q} is chosen to be less than 1.0 in the present study to ensure that the local sub-domains of the internal nodes are entirely within the solution domain, without being intersected by the global boundary. Theoretically, both ratios are very flexible [23].

As over-lapping sub-domains are used, the test-domain size (or local domain of integration/collocation) Ω_q affects the accuracy of the solution and the efficiency of the method. It is very different from the non-over-lapping methods, in which the background cells are required to partition the solution domain. For the applications presented in this paper, $\alpha_s = 2.0 \sim 3.0$ and $\alpha_q = 0.5 \sim 0.6$ were used. Only local meshless methods like the RBDMF, the GSMF and the MLPG FVM use local domains; the EFG use background cells for integration purpose.

Displacement and energy norms can be used for error estimation. These norms can be computed, respectively as

$$\|\mathbf{u}\| = \left[\int_{\Omega} \mathbf{u}^T \mathbf{u}\, \mathrm{d}\Omega\right]^{1/2} \tag{54}$$

and

$$\|\varepsilon\| = \left[\frac{1}{2}\int_{\Omega} \varepsilon^T \mathbf{D}\, \varepsilon\, \mathrm{d}\Omega\right]^{1/2}. \tag{55}$$

The relative error for $\|\mathbf{u}\|$ and $\|\varepsilon\|$ is given, respectively by

$$r_u = \frac{\|\mathbf{u}_{num} - \mathbf{u}_{exact}\|}{\|\mathbf{u}_{exact}\|} \tag{56}$$

and

$$r_\varepsilon = \frac{\|\varepsilon_{num} - \varepsilon_{exact}\|}{\|\varepsilon_{exact}\|}. \tag{57}$$

Now consider a beam of dimensions $L \times D$ and of unit depth, subjected to a parabolic traction at the free end as shown in Fig. 6. The beam is assumed in a plane stress state and the parabolic traction

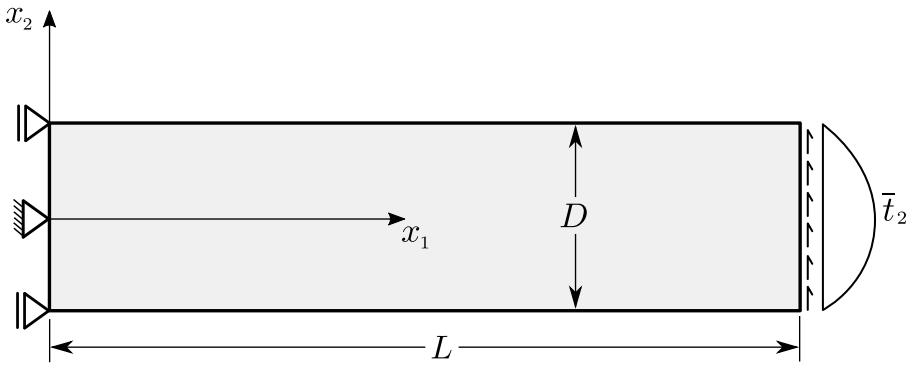

Figure 6. Timoshenko cantilever beam problem.

is given by

$$\bar{t}_2(x_2) = -\frac{P}{2I}\left(\frac{D^2}{4} - x_2^2\right), \tag{58}$$

where $I = D^3/12$ is the moment of inertia. The exact displacement components for this problem are given by

$$u_1(x_1,x_2) = -\frac{Px_2}{6EI}\left[(6L-3x_1)x_1 + (2+\nu)\left(x_2^2 - \frac{D^2}{4}\right)\right] \tag{59}$$

and

$$u_2(x_1,x_2) = \frac{P}{6EI}\left[3\nu x_2^2(L-x_1) + (4+5\nu)\frac{D^2 x_1}{4} + (3L-x_1)x_1^2\right] \tag{60}$$

and the exact stress components are given by

$$\sigma_{11}(x_1,x_2) = -\frac{P(L-x_1)x_2}{I}, \quad \sigma_{22}(x_1,x_2) = 0. \tag{61}$$

and

$$\sigma_{12}(x_1,x_2) = -\frac{P}{2I}\left(\frac{D^2}{4} - x_2^2\right) \tag{62}$$

Material properties are taken as Young′s modulus $E = 3.0 \times 10^7$ and the Poisson′s ratio $\nu = 0.3$ and the beam dimensions are $D = 12$ and $L = 48$. The shear force is $P = 1000$.

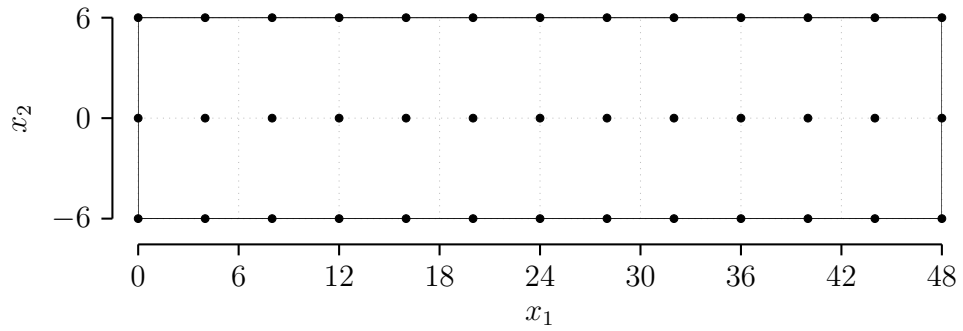

Figure 7. The regular nodal distribution of $13 \times 3 = 39$ nodes.

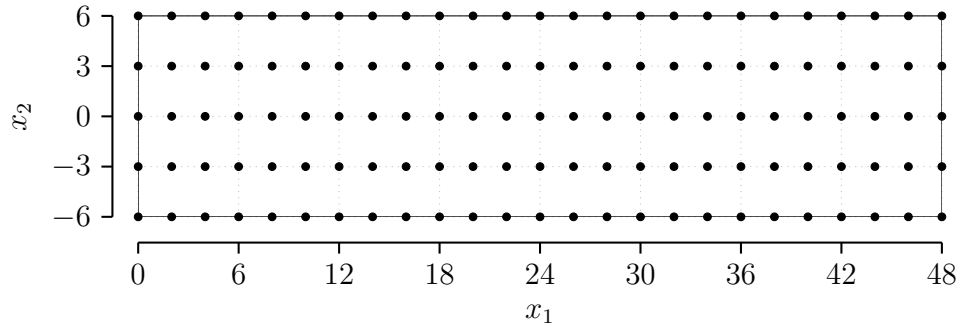

Figure 8. The regular nodal distribution of $25 \times 5 = 125$ nodes.

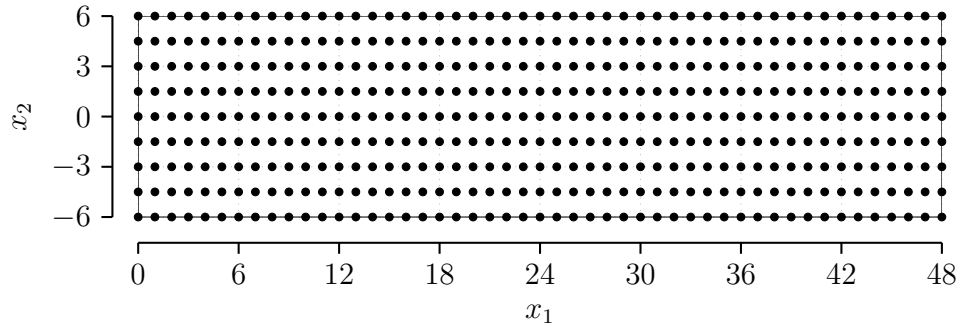

Figure 9. The regular nodal distribution of $49 \times 9 = 441$ nodes.

6.1 Displacement comparison

To solve this problem, three regular nodal distributions, represented in Fig. 7, Fig. 8 and Fig. 9, were considered, respectively with a discretization of $13 \times 3 = 39$ nodes, $25 \times 5 = 125$ nodes and $49 \times 9 = 441$ nodes.

For the local kinematic formulations, rectangular local domains were considered, with 1 collocation point to compute the weak form of GSMF and 10 Gauss-quadrature points to integrate the weak-form of RBDMF, placed on each boundary of the local domain. The EFG considered 10 Gauss-quadrature points on each background cell and the MLPG FVM considered 10 Gauss-quadrature points distributed on the local domain. A first-order polynomial basis was considered in MLS approximation for all methods.

The displacements obtained with the four methods, represented in Fig. 10 for the nodal distribution of 39 nodes, Fig. 11 for the nodal distribution of 125 nodes and Fig. 12 for the nodal distribution of 441 nodes, show very good agreement with the results of the exact solution, although the MLPG FVM is less accurate than the others. The best results are obtained with the nodal distribution of 441 nodes with a relative displacement error of $r_u = 9.52 \times 10^{-4}$ for GSMF, $r_u = 6.18 \times 10^{-3}$ for

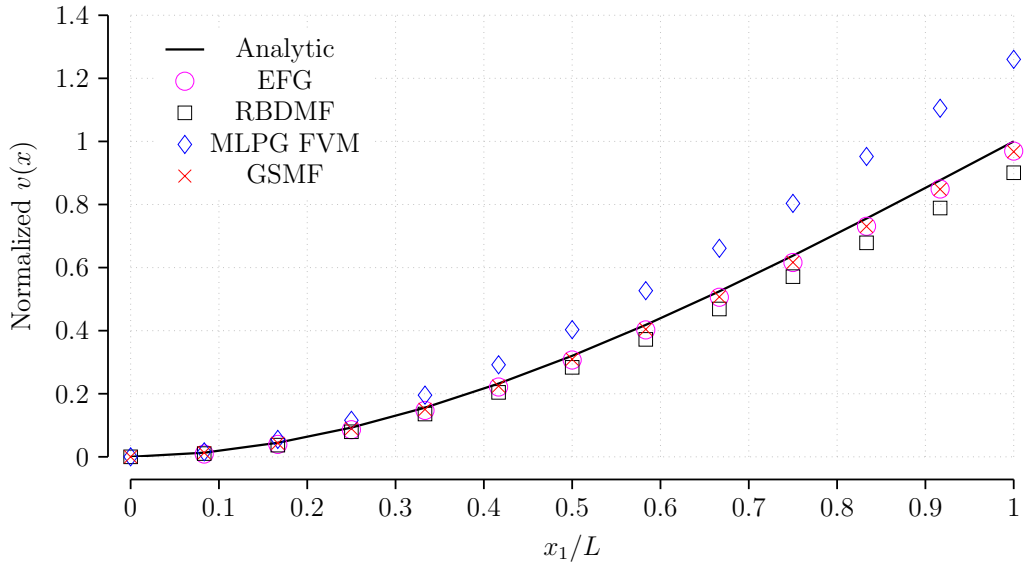

Figure 10. Normalized displacements of the cantilever-beam discretization with 39 nodes.

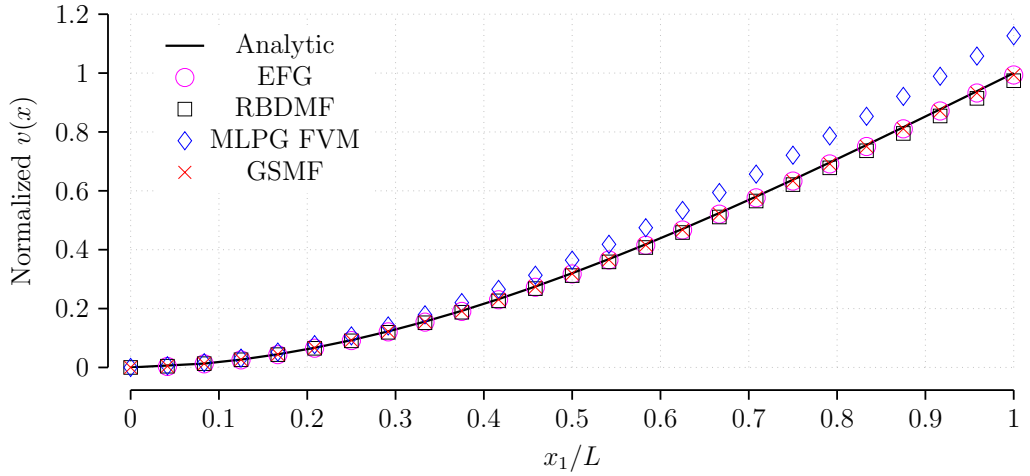

Figure 11. Normalized displacements of the cantilever-beam discretization with 125 nodes.

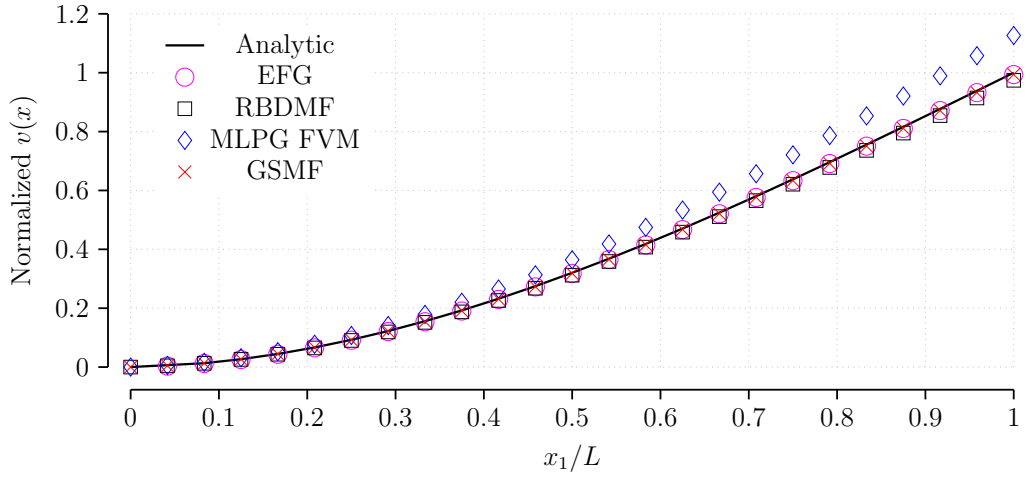

Figure 12. Normalized displacements of the cantilever-beam discretization with 441 nodes.

RBDMF, $r_u = 1.61 \times 10^{-3}$ for EFG and $r_u = 4.52 \times 10^{-2}$ for MLPG FVM. Considering the same nodal distribution used in this study, in [16] it can be seen that the MLPG FVM performs slightly

better when $c_i = 0.5 \sim 1$ and some of the beam properties are changed.

6.2 Computational efficiency comparison

The weak-form collocation of GSMF represents a clear reduction of the computational effort when compared to other meshless methods. The GSMF require only 1 collocation point, placed on each boundary of the local domain, to obtain the most accurate results, see [17]; while the other methods require at least 10 Gauss-quadrature points in order to obtain a good accuracy. This important feature is measure through CPU time consumption and convergence rates.

In order to further the study of the computational efficiency of the presented method, three regular discretizations with $13 \times 3 = 39$ nodes, $25 \times 5 = 125$ nodes and $49 \times 9 = 441$ nodes of the cantilever-beam were considered. Only the major computational cost that is the cost of generating the global stiffness matrix and solving the system of algebraic equations, was measured. All the routines were compared when using MATLAB 2015a on an Intel Core I7-4700MQ computer with CPU of 2.4GHz and 16 GB of RAM. The results obtained are presented in Table 1, where it can be seen that CPU

Table 1. CPU time measured.

Nodes	CPU time (s)			
	GSMF	MLPG FVM	RBDMF	EFG
39	0.071822	0.60317	0.549702	0.62397
125	0.273383	1.8586	2.093391	2.716241
441	1.130718	6.9303	8.904841	11.633007

time of GSMF is always much lower than CPU time of the other methods, using the same parameters. The CPU time consumption of the GSMF is 6.13 times faster than the second best value that is the one obtained with the MLPG FVM. This important result clearly evidences the high computational efficiency of GSMF.

6.3 Accuracy and convergence comparison

Another test was performed to assess the accuracy and the convergence rate of the analyzed methods, using the relative energy norm. Since the MLPG FVM obtained the least accurate result among all methods, it was not compared in this test. The same three regular discretizations of the cantilever-beam were considered. Figure 13 presents the results obtained for the accuracy and convergence rates,

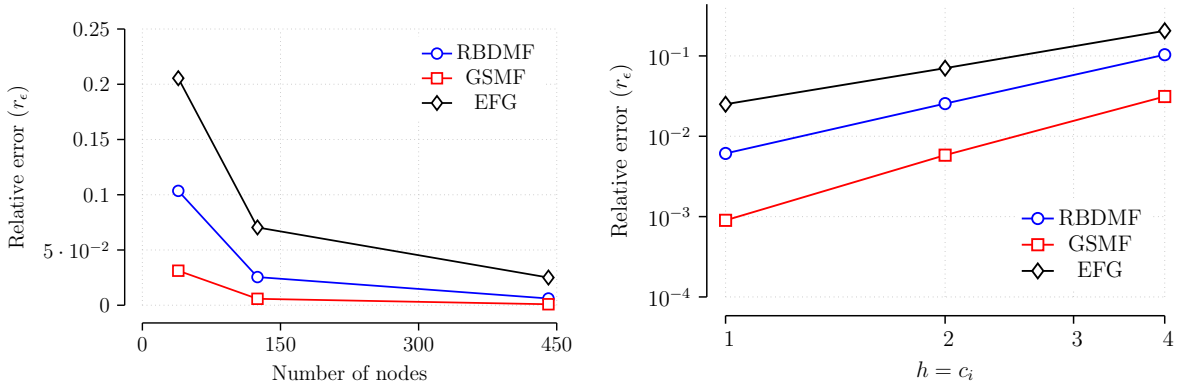

Figure 13. Accuracy and convergence rates respectively for the cantilever-beam discretization with 39, 125 and 441 nodes; c_i is the distance of a generic node i, to the nearest neighboring node, as defined in Eq. (52) and (53).

also in agreement with other comparative studies using different nodal distributions and properties

[24]. As expected, the best results are obtained with the nodal distribution of 441 nodes, with a relative error of $r_\varepsilon = 8.99 \times 10^{-4}$ for the GSMF, $r_\varepsilon = 6.11 \times 10^{-3}$ for the RBDMF and $r_\varepsilon = 2.51 \times 10^{-2}$ for the EFG. The results show that the GSMF is more accurate than the RBDMF and the EFG, with better convergence rates when compared to both of them.

7. CONCLUSIONS

A numerical comparison of the overall performance of the weak-form collocation and three meshless methods is performed, for for solving two-dimensional linear elastic problems.

While the Rigid-body Displacement Mesh-free (RBDMF) formulation, the Element-free Galerkin (EFG) and the Meshless Local Petrov-Galerkin Finite Volume Method (MLPG FVM) rely on integration and quadrature process to obtain the stiffness matrix of the posed problem; the Generalized-Strain Mesh-free (GSMF) formulation is completely integration free, working as a weighted-residual weak-form collocation.

A numerical example was analyzed with these methods, in order to compare the accuracy and the computational effort under the same parameters. The results obtained with all methods are in agreement with those of the available analytical solution. The MLPG FVM led to very fast computations, which are compromised by the low accuracy obtained. The EFG and the RBDMF obtained very accurate results with good convergence rates, although are computationally more expensive than the other methods. Among all methods, the GSMF excel, obtaining the most accurate results with the fastest computation.

All the numerical results obtained clearly demonstrate that this weighted-residual weak-form collocation readily overcomes the well-known difficulties posed by the weighted-residual strong-form collocation, regarding accuracy and stability of the solution. The results obtained using only 1 collocation point led to accurate results with incredible fast computations, surpassing all the other analyzed methods. This features make the GSMF superior when compared to the other meshless methods presented in this paper, making it a robust formulation for solving two-dimensional problems in linear elasticity.

Finally, it is expected that the GSMF framework will be implemented in a variety of problems, especially for large deformations, impact engineering and fracture mechanics, in the very near future.

8. ACKNOWLEDGEMENTS

The first author acknowledges the program *PECC – Pós-Graduação em Estruturas e Construção Civil*, Department of Civil and Environmental Engineering, Faculty of Technology, University of Brasília and *CNPq – Brazilian National Counsel of Technological and Scientific Development* for his PhD scholarship.

REFERENCES

[1] Liu, G. R. (2009). Meshfree methods moving beyond the finite element method. CRC Press, 2nd edition edition.

[2] Finalyson, B. A. (1972). The Method of Weighted Residuals and Variational Principles. Academic Press.

[3] Lucy, L. (1977). "A numerical approach to testing the fission hypothesis." Astronomical Journal, 82:1013–1024.

[4] Nayroles, B., Touzot, G., and Villon, P. (1992). "Generalizing the Finite Element Method: Diffuse Approximation and Diffuse Elements." Computational Mechanics, 10:307–318.

[5] Liu, W. K., Jun, S., and Zhang, Y. F. (1995). "Reproducing Kernel Particle Methods." International Journal for Numerical Methods in Engineering, 20:1081–1106.

[6] Belytschko., T., Lu, Y. Y., and Gu, L. (1994). "Element-free Galerkin methods." International Journal for Numerical Methods in Engineering, 37(2):229–256. ISSN 1097-0207.

[7] Atluri, S. N. and Zhu, T. (1998). "A new Meshless Local Petrov-Galerkin (MLPG) approach in computational mechanics." Computational Mechanics, 22(2):117–127.

[8] Atluri, S. N. and Shen, S. (2002). "The Meshless Local Petrov-Galerkin (MLPG) Method: A Simple and Less-costly Alternative to the Finite Element and Boundary Element Methods." CMES: Computer Modeling in Engineering and Sciences, 3(1):11–51.

[9] Zhu, T., Zhang, J., and Atluri, S. N. (1998). "A Local Boundary Integral Equation (LBIE) Method in Computational Mechanics and a Meshless Discretization Approach." Computational Mechanics, 21:223–235.

[10] Liu, G. R. and Gu, Y. T. (2001). "A Local Point Interpolation Method for Stress Analysis of Two-Dimensional Solids." Structural Engineering and Mechanics, 11(2):221–236.

[11] Liu, G. R., Yan, L., Wang, J. G., and Gu, Y. T. (2002). "Point Interpolation Method Based on Local Residual Formulation Using Radial Basis Functions." Structural Engineering and Mechanics, 14:713–732.

[12] Lin, H. and Atluri, S. N. (2000). "Meshless local Petrov–Galerkin (MLPG) method for convection–diffusion problems." CMES: Computer Modeling in Engineering and Sciences, 1:45–60.

[13] Lin, H. and Atluri, S. N. (2000). "The meshless local Petrov–Galerkin (MLPG) method for solving incompressible Navier–Stokes equations." CMES: Computer Modeling in Engineering and Sciences, 2:117–42.

[14] Atluri, S. N., Sladek, J., Sladek, V., and Zhu, T. (2000). "The local boundary integral equation (LBIE) and its meshless implementation for linear elasticity." Computational Mechanics, 25:180–98.

[15] Sladek, J., Sladek, V., and Atluri, S. N. (2000). "Local boundary integral equation (LBIE) method for solving problems of elasticity with nonhomogeneous material properties." Computational Mechanics, 25:456–62.

[16] Atluri, S. N., Han, Z. D., and Rajendran, A. M. (2004). "A New Implementation of the Meshless Finite Volume Method Through the MLPG Mixed Approach." CMES: Computer Modeling in Engineering and Sciences, 6:491–513.

[17] Oliveira, T. and Portela, A. (2016). "Weak-Form Collocation – a Local Meshless Method in Linear Elasticity." Engineering Analysis with Boundary Elements, 73:144–160.

[18] Fredholm, I. (1906). "Solution d'un probléme fondamental de la théorie de l'élasticité." Arkiv för Matematik Astronomi och Fysk 2, 28(1):1–8.

[19] Fichera, G. (2006). Linear Elliptic Differential Systems and Eigenvalue Problems. Springer.

[20] Brebbia, C. A. and Tottenham, H., editors. Variational Basis of Approximate Models in Continuum Mechanics. Southampton and Springer Verlag.

[21] Sokolnikoff, I. S. (1956). Mathematical theory of elasticity. McGraw-Hill New York.

[22] Gelfand, I. M. and Shilov, G. E. (1964). Generalized Functions, volume 1. Academic Press.

[23] Han, Z. and Atluri, S. N. (2011). "A Truly-Meshless Galerkin Method, though the MLPG mixed approach." Journal of Marine Science and Technology, 19(4):444–452.

[24] Oliveira, T. and Portela, A. (2016). "Comparative Study of the Weak-Form Collocation Local Meshless Formulation and other meshless methods." In Proceedings of the XXXVII Iberian Latin-American Congress on Computational Methods in Engineering. Brasilia, Brazil.

RESPONSIBILITY NOTICE

The authors, Tiago Oliveira and Artur Portela, are the only responsible for the printed material included in this paper.